Colloids and Surfaces B: Biointerfaces 190 (2020) 110971

Contents lists available at ScienceDirect

Colloids and Surfaces B: Biointerfaces

journal homepage: www.elsevier.com/locate/colsurfb

Effect of substrate topography on the regulation of human corneal stromal cells

Promita Bhattacharjee[a,b], Brenton. L. Cavanagh[c], Mark Ahearne[a,b,*]

[a] Trinity Centre for Biomedical Engineering, Trinity Biomedical Sciences Institute, Trinity College Dublin, University of Dublin, Dublin, Ireland
[b] Department of Mechanical and Manufacturing Engineering, School of Engineering, Trinity College Dublin, University of Dublin, Dublin, Ireland
[c] Cellular and Molecular Imaging Core, Royal College of Surgeons in Ireland, Dublin, Ireland

ARTICLE INFO

Keywords:
Morphology
Keratocytes
Cell migration
Cell adhesion
Biomaterial
Microgrooves

ABSTRACT

Optimal functionality of native corneal stroma depends on a well-ordered arrangement of extracellular matrix (ECM). To develop an *in vitro* corneal model, replication of the corneal *in vivo* microenvironment is needed. In this study, the impact of topographic cues on keratocyte phenotype is reported. Photolithography and polymer moulding were used to fabricate microgrooves on polydimethylsiloxane (PDMS) 2–2.5 μm deep and 5 μm, 10 μm, or 20 μm in width. Microgrooves constrained the cells body, compressed nuclei and led to cytoskeletal reorganization. It also influenced the concentration of actin filaments, condensation of chromatin and cell proliferation. Cells became more spread and actin filament concentration decreased as the microgroove width increased. Relationships were also demonstrated between microgroove width and cellular processes such as adhesion, migration and gene expression. Immunocytochemistry and gene expression (RT-PCR) analysis showed that microgroove width upregulated keratocyte specific genes. A microgroove with 5 μm width led to a pronounced alignment of cells along the edges of the microchannels and better supported cell polarization and migration compared with other microgroove widths or planar substrates. These findings provide important fundamental knowledge that could serve as a basis for better-controlled tissue growth and cell-engineering applications for corneal stroma regeneration through topographical patterns.

1. Introduction

Cell behavior can be affected by their surrounding physical environment. Understanding the response of cells to different structural and topographical cues needs to be considered when developing materials that directly interact with cells for applications such as medical implants, cell culture systems or scaffolds for tissue engineering. Several cell types have previously been shown to modulate their behavior in response to changes in surface topography *in vitro* [1–4]. As an example, topographical patterns consisting of microscale grooves and ridges have been shown to encourage cell alignment [5]. The spatial and temporal patterns shown by cell colonies during tissue growth are a result of cell-cell interaction, influence of extracellular forces, cell movement and coordinated cell growth. Hence, these patterns play an important role in organ development [6].

Our understanding of how cells imbibe topographic signals remains incomplete. Cell responses can vary depending on the specific topographical pattern. Within organs and tissue, the microenvironment surrounding cells also presents structural constraints that influence the regulation of cellular functions [7–10]. Cell geometry affects nuclear deformation, cytoskeleton organization, gene expression, cell growth and apoptosis, cell division and chromatin compaction [11–13]. Similarly, other biophysical cues in the cell's microenvironment (*e.g.*, fluid flow, substrate stretching and rigidity) affect gene expression and cellular and nuclear architecture [14–16]. While the impact such parameters have on cellular function remains obscure, multiple studies unequivocally confirm that the topography of the cells microenvironment is critical in regulating their behavior [17–19]. Several *in vitro* studies have shown that patterns on the substrate impact cell adhesion, differentiation, and migration [20]. The biophysical and biochemical stimuli influencing cell behavior have been linked to substrate-cytoskeleton crosstalk [21].

The corneal stroma is dependent on a high degree of structural organization to maintain its transparency and mechanical characteristics. The extracellular matrix (ECM) structure and composition are maintained by resident corneal stromal cell called keratocytes [22]. These

* Corresponding author at: Trinity Centre for Biomedical Engineering, Trinity Biomedical Sciences Institute, Trinity College Dublin, University of Dublin, Dublin, Ireland.
E-mail address: ahearnm@tcd.ie (M. Ahearne).

https://doi.org/10.1016/j.colsurfb.2020.110971
Received 20 November 2019; Received in revised form 17 February 2020; Accepted 11 March 2020
Available online 12 March 2020

cells interact with each other, the surrounding ECM and nerve fibers [5]. The ECM primarily consists of collagen aligned fibrils 22.5 nm–35 nm in diameter with a center-to-center gap of approximately 62 nm. These fibrils form lamella of thickness 2 μm–200 μm [23] in between which the keratocytes reside. Nerve fibers are mostly limited to the anterior stroma where they are in the form of bundles of up to 20 μm diameter [5] and run parallel to the collagen fibrils. The combination of these different microstructural features in the stroma likely influence how keratocytes behave.

Substrate topography, through contact guidance can strongly impact keratocytes. Arrays of parallel grooves and ridges, in nano and micro dimensions, have previously been used to models *in vivo* ECM architecture of the corneal stroma. Substrate topographic cues have been known to affect orientation of stromal cells and orientation and elongation of keratocytes. A study by Teixeira et al. [5] on silicon substrates with groove pitches between 400 and 4000 nm showed that for pitches over 800 nm, 70 % of human keratocytes were elongated and aligned along the grooves. Studies have also shown ridges and grooves affecting keratocyte migration and morphology in rabbit cornea [22]. Irrespective of surface chemistry, human corneal keratocytes were shown to proliferate more as ridge width increased from 0.35 to 10 μm [24]. Corneal keratocytes have been shown to slow down in their proliferation rate on nano scaled grooves, compared to microscale grooves and smooth substrates [25]. Koo et al. [24] also observed, primary human keratocytes proliferated slower with decreased groove width. Zhang et al. [26] used a biomimetic 3D corneal model, made up of patterned silk films and collagen gel to show that the topography of the silk films affected keratocyte alignment and ECM arrangement. The 3D model showed higher expression of keratocyte marker and expression of ECM compared to the 2D culture and the dome shaped model, with 3% strain showed higher expression of keratocyte marker.

To better understand how keratocytes respond to different topographical cues, microstructured substrates with microgrooves and microridges were fabricated using polydimethylsiloxane (PDMS). During tissue development and growth, cell colonies exhibited a variety of spatial and temporal patterns, as an outcome of coordinated cell growth, movement, and cell–cell communications. Here we show that geometrical confinement, induced by topographically patterned microgroove substrates, modulated cell and nuclear morphology and cellular behaviors like alignment, orientation, and migration. These factors are critical for biological phenomenon like embryogenesis, wound healing, metastasis, inflammation, and colonization of biomaterial scaffolding [20]. The results indicate that the topographic constraints significantly squeezed the cells and nuclei, increased chromatin condensation – leading to changed cell proliferation rate – and cytoskeleton reorganization and anisotropic growth of the cultures. The role played by filopodial probing (adhesion establishment, focal adhesion orientation), cell environmental sensing, and growth in perception of and reaction to surface topographic features were also investigated.

2. Materials and methods

2.1. Fabrication of micro-patterned substrates

Micro-patterned silicon master molds were fabricated under cleanroom conditions as described earlier [27]. Briefly, molds were fabricated by standard soft lithography using a laser mask writer (Heidelberg DWL66), reactive ion etching and low-pressure chemical vapor deposition for silicon oxide coating. The molds had straight, parallel microgrooves made of photoresistant material. There were three master molds, each 1 × 1 cm in dimension: a) 5 μm microchannels with 5 μm spacing b) 10 μm microchannels with 10 μm spacing and c) 20 μm microchannels with 20 μm spacing. Dry plasma etching (OIPT Plasma lab System100 ICP180) was used to etch the master molds. 15 min of etching was utilized to achieve the depth of microchannels. Micropatterned polydimethylsiloxane (PDMS) substrates were fabricated by mixing elastomer base and curing agent (10:1 ratio by weight). The elastomer solution was degassed and poured on the master molds. The molds were then cured for 24 h, at 60 °C. Control (non-patterned) substrates were fabricated by casting the elastomer solution on a 60 mm polystyrene Petri dish (Corning, Corning, NY, USA), followed by the same curing. A schematic overview of the fabrication process has been provided Supplementary Fig. 1.

The PDMS patterned substrates (1 cm × 1 cm) were characterized by scanning electron microscopy (SEM, SUPRA 35 V P, Carl Zeiss) and white light interferometry (Omniscan MicroXam-non-contact optical method) to measure the surface roughness (RMS: root mean square) and the depth of microgrooves channels.

2.2. Cell culture

Human corneal stromal cells at passage 3 were used in this study. The cells were isolated for use in this study as previously describe [28] in accordance with the declaration of Helsinki and with ethical approval from Trinity College Dublin School of Medicine Research Ethic Committee. The culture medium used to expand cells was comprised of Dulbecco's Low Glucose Modified Eagles Medium (DMEM) (Hyclone; Thermo Fisher Scientific) supplemented with 10 % fetal calf serum (Hyclone) and 1 % penicillin/streptomycin. The culture took place in a controlled, humidified environment (5 % CO_2, 37 °C) until cells reached 90 % confluency. At this point, cells were trypsinized and centrifuged to be counted while suspended in the media. Cells were stained (Trypan Blue) and counted using a Haemocytometer. The patterned substrates (1 × 1 cm^2) were sterilized by UV exposure (30 min) and soaked in low glucose DMEM medium for 4 h. The matrices were then partially dried before cell seeding.

10 μL of cell suspension in media, containing 10^3 cells, were seeded dropwise onto each matrix. The matrices were maintained in a humidified environment, at 37 °C and 5 % CO_2 for 1 h after seeding. Culture medium was added to the cell seeded substrates consisting of DMEM/F12 (Hyclone; Thermo Fisher Scientific) supplemented with L-ascorbic acid (0.1 mM), Insulin-Transferrin-Selenium (Gibco) (1 μl/ml), and 1 % penicillin/streptomycin. Media was replaced on every alternate day.

2.3. Cellular proliferation

Cell proliferation was assessed at multiple time-points over the 21 day culture period using PrestoBlue reagent (Molecular Probes; Invitrogen, Carlsbad, CA), following the manufacturers protocol.

2.4. Cytoskeletal organization

To observe cytoskeletal organization, following 3 days of culture, cell laden substrates were fixed with 4% paraformaldehyde for 15 min at room temperature. Cells were permeabilized with 0.1 % Triton X-100 solution in 1 % bovine serum albumin (BSA) and then blocked with 2 % BSA for 1 h. Phalloidin-TRITC and 4′,6 -diamidino-2-phenylindole (DAPI) were used to stain actin filaments (F-actin) and cell nuclei, respectively. For both stains, respective manufacturer's protocols were followed. Leica SP8 confocal microscope was used to examine the cytoskeletal organization on the matrices with LAS X Advanced software being used for image post-processing.

F-actin alignment and density distribution were analyzed. A pseudo color scale was used to present the F-actin distribution fluorescence and intensity [11].

F-actin and DAPI staining were used to outline the cell perimeter and to calculate the cell and nucleus areas [29]. Analyze Particles, from Fiji [30] was used to quantify these areas. At each time point, for each substrate, 30 cells were analyzed.

2.5. Analysis of elongation and degree of orientation

The elongation and orientation of TRITC-phalloidin stained cells were measured 4, 12, and 24 h after initial seeding as previously described [13]. Cell elongation was defined as the ratio of the maximum to the minimum principal moment of inertia (Supplementary Fig. 2). Cell orientation was defined as the angle (θ) between the principal axis of inertia of the elliptical form and a reference axis. θ varied between 0 and 180°. For reference axis, the pattern direction was used in the micro-grooved surfaces while the horizontal axis was used for the control surfaces (no grooves) – Schematic in Fig. 3. When θ exceeded 10°, cells were considered to have random orientation and were otherwise considered to be aligned.

2.6. Focal adhesions (FAs) and morphometric analysis

Vinculin staining was used to analyze focal adhesion. 12 h after cell seeding, cell-laden constructs were fixed and permealized as described earlier and then incubated with mouse monoclonal anti-vinculin antibody (Abcam) (1:400 dilution) overnight at 4 °C. The following day, substrates were washed thrice with PBS, 5 min per wash. Washed substrates were incubated in Alexa fluor-488-conjugated rabbit anti-mouse IgG (Abcam) – incubation in 1:200 dilution, for two hours at 37 °C. Actin and nucleus was counter stained as described previously. Substrates were then again thoroughly washed with PBS followed by confocal microscopy: Leica SP8 for imaging and LAS X Advanced for image post-processing.

The methodology from Maruoka et al. was used for FA morphometric analysis (length *vs* orientation) [31]. Only FAs with area over 0.6 mm^2 were part of the statistical analysis. ImageJ command "Measure" was used to measure FA length. FA lengths (n = 60) were analyzed with respect to pattern orientation.

2.7. Apparent chromatin condensation

DAPI staining was used to visualize chromatin and to analyze the spatial chromatin organization. Nuclear images at different focal positions along the z-axis, every 0.2 mm interval, were acquired using confocal scanning microscopy (Leica SP8) and stacked. Images were sharpened with ImageJ plugins (shading correction, dark image subtraction, Deconvolution Lab) to extract quantitative information from them. As the sum of the intensity of each pixel, the integrated fluorescence intensity was quantified. The average spatial density is the ratio of total fluorescence intensity to nuclear volume and correlates with average chromatin packing ratio [13]. It is indicative of chromatin condensation.

2.8. Filopodia feature analysis through SEM

Cell laden substrates were fixed (4 % PFA, 15 min, room temperature) and filopodia examined 24 h after seeding. Cells were subjected to graded dehydration steps using ethanol (30–100 % v/v H_2O, steps of 10 %, 20 min. in each). Dehydrated samples were exposed to isoamyl acetate for 5 min, followed by vacuum drying and gold coating for scanning electron microscopy (SEM, Zeiss Sigma 300, operating voltage of 10 kV).

2.9. Cell migration analysis

4 h after initial seeding, cell migration was monitored over a further 6 h. The study focused on early intervals following seeding since the cell density is low during this period, helping us avoid the impact of cell-cell interactions. Six representative areas of each substrate were selected. DIC images were then acquired of each area using an EC Plan-Neofluar 10x (N.A. 0.3) objective every 15 min on a Carl Zeiss AxioImager Z1 (Jena, Germany) equipped with environmental enclosure and CO_2 and hardware autofocus. Time-lapse videos were manually analyzed with Track mate Plugin of Fiji. This analysis yielded cell trajectories. Mean migration rate was defined as the total movement of the call per unit time and directionality was assessed as movement across *vs* movement along pattern direction [18].

2.10. Gene expression by real-time real Time-PCR

Real-time reverse transcription PCR was used to quantify relative gene expression. This was carried out after 21 days of culture following protocol in literature [32]. Gene expressions were normalized using the ΔΔCt method, against GAPDH and flat substrate. The gene expression values thus calculated were expressed as an exponential in the form of $2^{-\Delta\Delta Ct}$. The primers (Applied Biosystems, Biosciences, Dublin, Ireland) evaluated were: αSMA (Hs00426835_g1), ALDH3A1 (Hs00964880_m1), decorin (DCN;Hs00754870_s1), glyceraldehyde-3-phosphate dehydrogenase (GAPDH; Hs02758991_g1), keratocan (KERA;Hs00559942_m1), and lumican (LUM; Hs00929860_m1), collagen type III (COL3A1; Hs00943809_m1), collagen type I (COL1A1; Hs00164004_m1), collagen type V (COL5A1; Hs00609133_m1_m1).

2.11. Evaluation of Extracellular Matrix (ECM) characterization and matrix stiffness

ECM formation on the cell laden substrates and the culture media was quantified using biochemical analysis after 14 and 28 days of culture period. Bisbenzimide Hoechst 33258 DNA assay with calf thymus DNA was used as the reference standard for quantifying DNA content [33]. Cells on substrates were macerated by a papain solution (125 μg/ml). Dimethyl methylene blue (DMMB) binding assay (Blyscan; Biocolor Ltd, Antrim, UK) was performed to determine levels of sGAG (acid sulfated glycosaminoglycans), standard used was bovine chondroitin sulfate. Matrix stiffness of all substrates after 7 days of culture was evaluated by contact mode atomic force microscopy (AFM-Park NX10) using force-displacement curve (Park Systems XEI software) [34]. Standard triangular silicon nitride cantilevers from Veeco (DNP) with a nominal spring constant of 0.06 N/m and a nominal tip radius of curvature of 20 nm were used. The XEI software calibration tool was utilized to measure the cantilever spring constant. The AFM was run in the force-volume mode at frequency of 7 Hz to obtain force distance curve.

2.12. Immunocytochemistry

Following 14 days in culture, cell-laden substrates were pre-processed for immunocytochemistry analysis using the same method as for F-actin staining. After permeabilization and blocking, cells were incubated at 4 °C in anti-ALDH3A1 1:50 (ab76976; Abcam, Cambridge, United Kingdom), anti-keratocan 1:50 (sc-66941; Santa Cruz, Heidelberg, Germany), and anti-α-smooth muscle actin (αSMA) 1:50 (ab7817; Abcam) for 18 h. The cells were then thoroughly washed with PBS. They were then incubated for one hour, at room temperature, in a dark room, in fluorescently labelled antibodies. To detect Keratocan and ALDH3A1, Donkey anti-rabbit AlexaFluor 488 (ab150073; Abcam) was used. For αSMA, goat anti-mouse biotin was used, succeeded by Extr Avidin-FITC (B7151 and E2761). For nuclear staining, the substrates were then washed with PBS and incubated with DAPI (1 mg/mL,1:500 dilution). Confocal microscopy was carried out using the Leica SP8 and post-processing used LAS X Advanced software.

2.13. Statistical analysis

The R statistical platform was used for all statistical analysis. One-way ANOVA, followed by Tukey's post-hoc HSD test was used for comparing the results from different substrates. Significant differences have been marked as ***$p < 0.001$; **$p < 0.01$; *$p < 0.05$. Data

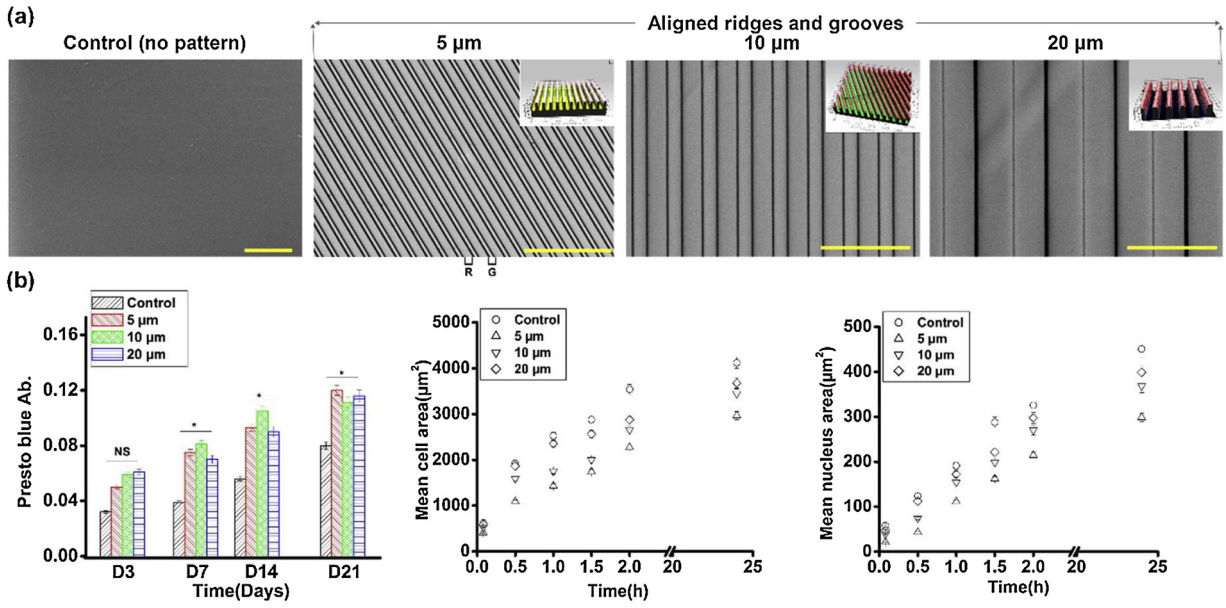

Fig. 1. Substrates with micro patterned surfaces for cell culturing: (a) Scanning electron micrographs of different PDMS substrates with aligned microgrooves; Scale bar = 50 μm. (b) substrate topography affected cell proliferation and mean cell and nucleus area. Data presented as mean ± SD, n = 20, (*p < 0.05).

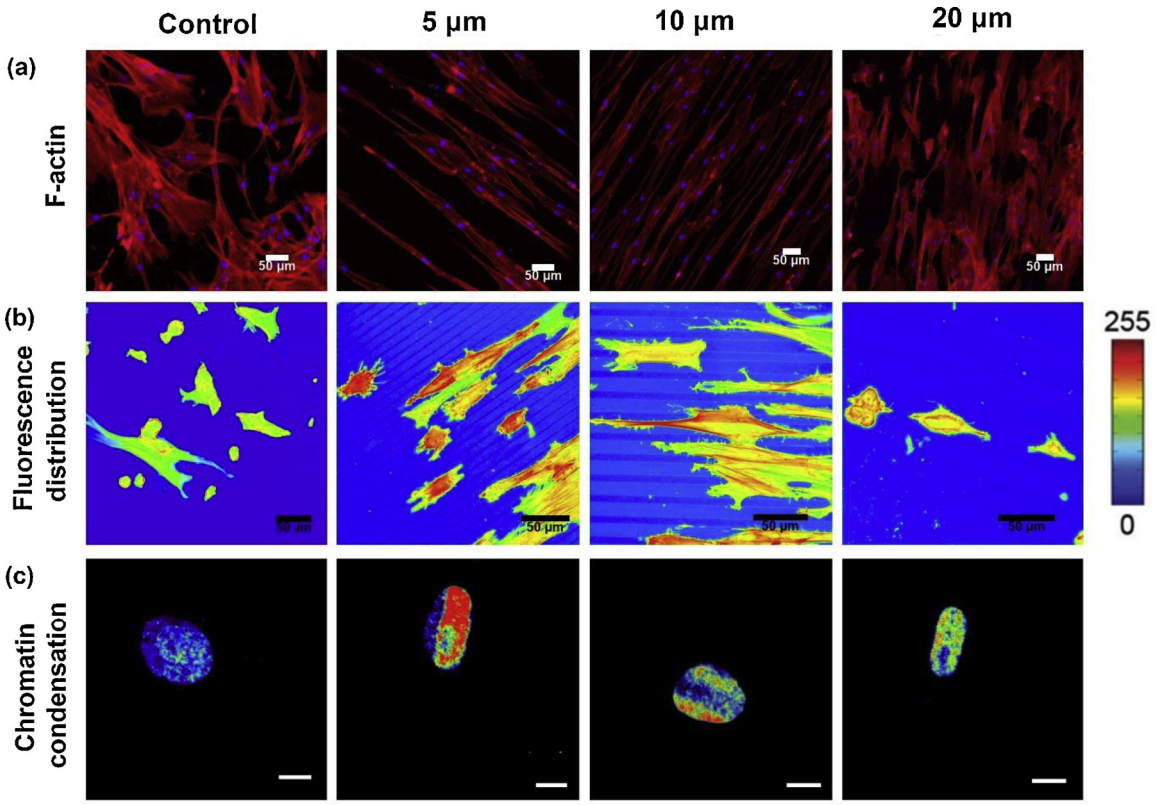

Fig. 2. Representative images of cells grown for 3 days on different PDMS patterned substrates. The fluorescence distribution and intensity of F-actin are shown in the reported pseudo-color scale (0-255). Intensities of DNA staining were digitized in 256 bits and colour coded. Highly condensed domains showed higher fluorescence intensity. (scalebar (a, b) = 50 μm, (c) = 8 μm).

presentation is in the form mean ± standard deviation (SD). Unless otherwise specify, sample size was 3.

3. Results

3.1. Substrate characterization

To study the cell response to aligned topography, PDMS substrates with aligned micro-grooves were fabricated. To verify pattern transfer, SEM was used to inspect the groove and channel width (Fig. 1(a)). The

grooves were of expected size (5 μm, 10 μm and 20 μm) and no defects were detected on the surface. The tops 10 μm and 20 μm ridges were also of expected size, although the 5 μm were slighty smaller (≈ 4.6 μm) due to the sides of the groove not being completely vetical. White light interferometry was used to evaluate depth of the channels (15 min plasma etching, ~2 μm to 2.5 μm) and their average surface roughness (RMS ~ 275 – 305 nm).

3.2. Cell proliferation and size changes in response to the substrate topography

The cells growth kinetics were studied over 21 days (Fig. 1(b)). Cell numbers increased linearly with time on all substrates. After 3 days, cell growth kinetics did not differ significantly between patterned substrates and control substrates. On days 7, 14 and 21 the patterned substrates had significantly more cells than the control. There was no significant difference in proliferation between cells on the different sized microchannels over 21 days.

Cell size affects vital cellular processes such as growth, morphology, differentiation and death [13]. Cells grown on micro-patterned substrates were significantly (*$p < 0.05$) smaller than those on the control. The nuclei of cells on patterned substrates were also significantly smaller (*$p < 0.05$) than the nuclei of cells grown on the control substrates. This finding is relevant in the context of the proposed mechanistic coordination between cell size, nuclear size [13] and cell cycle times [35].

3.3. F-actin network remodelling

Modulation of the F-actin network (*e.g.*, cross-linking density, length) will have an impact on cell shape and size [36–39]. It was observed that for the patterned substrates, the density of the actin filaments was affected, indicating a change in the cytoskeletal tension of the cultured cells. The representation in Fig. 2 uses colour coding (from blue to red) to show increasing density of F-actin. The actin density was noticeably high for the 5 μm patterned substrates compared to the other substrates. The length of actin filaments on the patterned substrates was also higher than on the plain substrates. Topographic cues present on microgroove substrates altered the cells shape that in turn influenced the stress fibre redistribution.

3.4. Chromatin condensation affected by substrate topography

DAPI staining was used to investigate effect of topographical cues on cell size and shape [11,40]. DAPI uptake levels were correlated to total DNA and its condensation level [41]. The ratio between integrated fluorescence intensity and nucleus volume may be considered an average spatial density that can be used as a reliable indicator for average chromatin condensation [9,37]. Fluorescence intensity increased in proportion to chromatin condensation level. Chromatin distribution reorganization was found to be associated with decreasing microgroove separation, least for the 5 μm patterned substrates. Nuclear reshaping was found to be associated with intense levels of chromatin condensation. The topographical cues led to the remodelling of cell as well as nuclear shape and resulted in reduced nuclear area.

3.5. Impact of substrate topography on cellular degree of orientation and alignment

Previous works have shown that cell organelles like centrosome, nucleus, and Golgi apparatus can orient themselves responding to external, physical stimuli [42,43]. At 4, 12, and 24 h following cell seeding, the orientation of the cell (nucleus) major axis was measured with respect to the pattern orientation on the substrate (Fig. 3a). The cell major axis is defined as the principal axis of the moment of area of the cell's two-dimensional projection. The cells on the patterned substrates significantly changed their nuclear and actin orientation, compared to those on the plain surface that lacked any specific orientation (Supplementary Fig. 3a). 4 h after seeding, cells on 5 μm (~36.2 %) and 10 μm (~23.3 %) grooved substrates had more readily oriented themselves along the pattern, compared to the 20 μm (~16.6 %) pattern substrates (Fig. 3b). Over time the cells on microgroove substrates became more orientated along the direction of the grooves. Nuclei orientation corresponded to the substrate topography's orientation. Cell

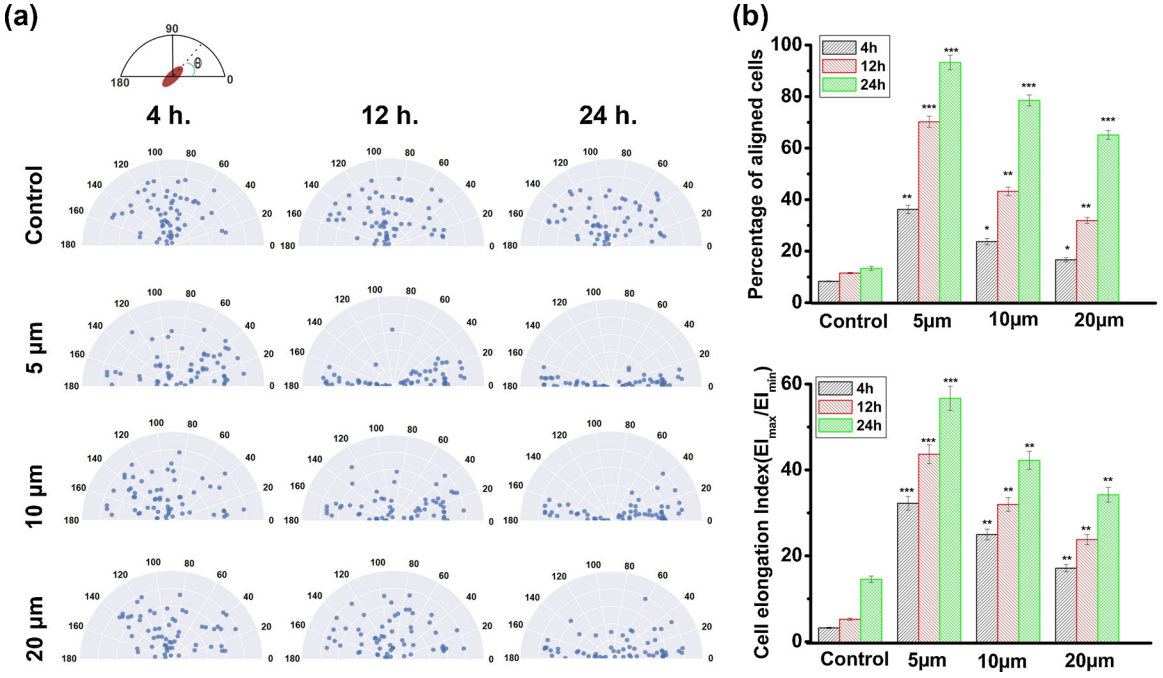

Fig. 3. (a) Substrate topography induced orientation of nucleus. Angular graphs show the different orientations experienced by nuclei (n = 60) in response to cell shape changes for different substrate topographies. (b) Histograms of the cell orientation at different cultured times with respect to the pattern direction and cell elongation index with time. Cells were considered aligned if the angle between the long axis and the patterns was 10° or less.

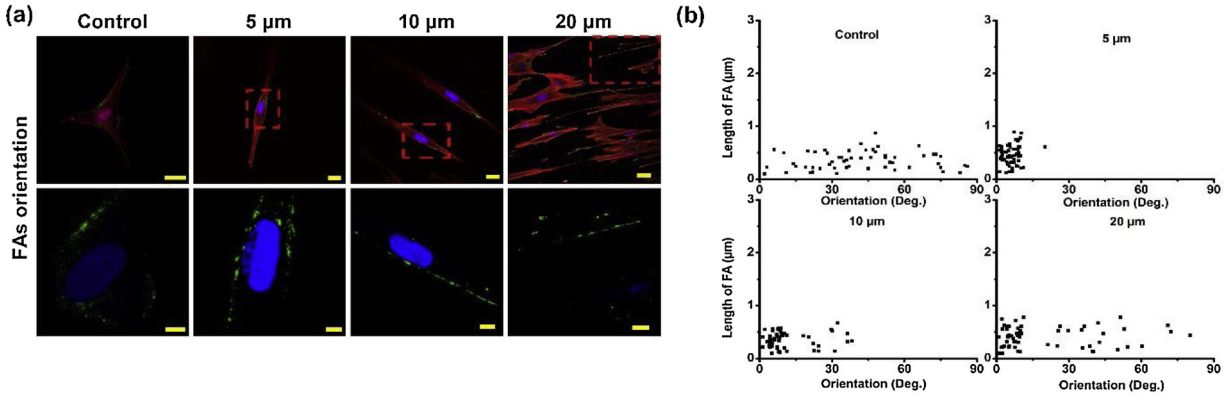

Fig. 4. (a) Focal adhesion (FA) orientation on different micropatterned substrates, after 12 h of culture period (scalebar = 20 μm). Cells were stained for actin fibres (red), vinculin (green) and nuclei (blue). On patterned substrates, FAs extend in the pattern direction. Their lengths were greater than ridge dimension. FAs are observed in a dashed and stable conformation, favoring cell elongation along the patterns. (b) Distribution of FA length (n = 60) with respect to pattern direction (scalebar = 5 μm). For flat substrates, the calculation was performed with respect to the horizontal axis. (For interpretation of the references to colour in the Figure, the reader is referred to the web version of this article).

elongation (n = 60) was noticeable on the patterned surface 12 h after seeding. On the plain surface, cells were less elongated compared to patterned substrates although some elongation occurred after 24 h. At this time-point, cells on the 5 μm substrates had the highest CEI (~56.68), followed by 10 μm (~42.23) and 20 μm (~34.21) substrates. At 4 h, cells were less elongated than at 24 h for all substrates. The patterned surfaces provided topographic cues that could prompt cell elongation and over shorter time duration than they would occur on a plain substrate.

3.6. Focal adhesion

Vinculin staining was used to identify FAs (Fig. 4a). There was a clear difference in the FAs between cells on the patterned and plain substrates. However, not all cells on the patterned surfaces had the same amount of FAs (Supplementary Fig. 3b). 12 h after seeding, vinculin was diffuse in the cell cytoplasm. FAs on the plain surfaces lacked any defined orientation while those on patterned surfaces were longer, located along the top of ridges and directed in the groove direction. This was more noticeable for the 5 μm and 10 μm substrates when compared to the 20 μm substrates (Fig.4a).

FA lengths, distributed for the different pattern orientations have been presented in Fig. 4b. For the different substrates, the FA length and their spatial distribution was different. After 12 h in culture, cells on all substrates exhibited FAs. Cells on 5 μm and 10 μm substrates displayed the most oriented and longest FAs.

3.7. Characteristics of filopodia on different patterned substrates

Filopodial probing, FA establishment and growth are the precursors to cell spreading and elongation. On the plain substrates, the filopodia were straight, while they were more bent on the patterned substrates. The bending was to allow the cells to follow the pattern direction (Fig. 5a). For the different microgroove substrates, the average filopodia length was not significantly different (Fig. 5b). The average length did not exceed 7.8 ± 1.4 μm while most of the filopodia were under 5 μm in length. This seems to imply that length scales of filopodial probing may be independent of surface micropatterns.

3.8. Direction of cell migration by topographic features

As topographic cues affected FA maturation, spatial distribution, cell orientation and elongation, it would be logical to assume that the surface microgrooves may also affect cell migration. Cell migration rates were analyzed through time-lapse images of the surfaces. For each substrate examined, 6 cells were tracked as they moved over the 6 h period. The starting point of each cell was mapped onto the origin (0,0) of the coordinate system used for plotting the cell positions (Fig. 6a). Cell migration trajectories on the plain substrate were isotopically distributed. For the patterned substrates, there was a correlation between cell trajectory and pattern orientation. This co-alignment was most conspicuous for the cells on the 5 μm pattern. Mean cellular migration rate was significantly higher on the patterned substrates, than on the plain substrate ($p < 0.001$, Fig. 6b). Among the patterned substrates, the 5 μm patterned substrate's mean cellular migration rate was remarkably high (~24.64 μm/h). The values for the 10 μm and 20 μm substrates were not significantly different.

3.9. Characterization of ECM

Corneal tissue generation requires that cells synthesize and secrete ECM that is specific to cornea. The most common, negatively charged macromolecules found in the corneal-stromal ECM are glycosaminoglycan (GAG) polysaccharides. Under normal circumstances, they are attached to proteoglycan core proteins by a covalent bond. Their contribution towards corneal transparency, nerve growth cone guidance, and cell adhesion can be critical [44]. GAG synthesis from the cells cultured on the different substrates were significantly higher for the patterned substrates, compared to the plain control, at day point (Fig. 7a). GAGs like chondroitin sulphate and keratan sulphate have a necessary role on controlling inter-fibril distances and transparency of the cornea [45]. After 7 days of culture, it was noted that the GAG deposits had stiffened the substrates (Fig. 7b) and this was significantly more for the patterned substrates than for the plain substrates. Stiffness for all substrates was recorded before seeding cells and it was similar (~25 ± 3.85 MPa) for all substrates.

3.10. Immunofluorescent staining and gene expression

After 21 days of culture, RT-PCR was used to quantify the gene expression (Fig. 8). Presence of micropatterns on the substrate led to increased expression of the keratocyte markers ALDH3A1, Keratocan, Decorin and Lumican, compared to the plain substrates. Collagen types I, III, and V are the most common collagen components of corneal stroma and all three had significantly higher levels of expression for the patterned substrates after 21 days in culture. Negative expression of αSMA (ACTA2) was recorded for all of the substrates at day point 21. This, in addition to the results from the immunocytochemical straining, implies that myofibroblastic differentiation was inhibited on all the substrates.

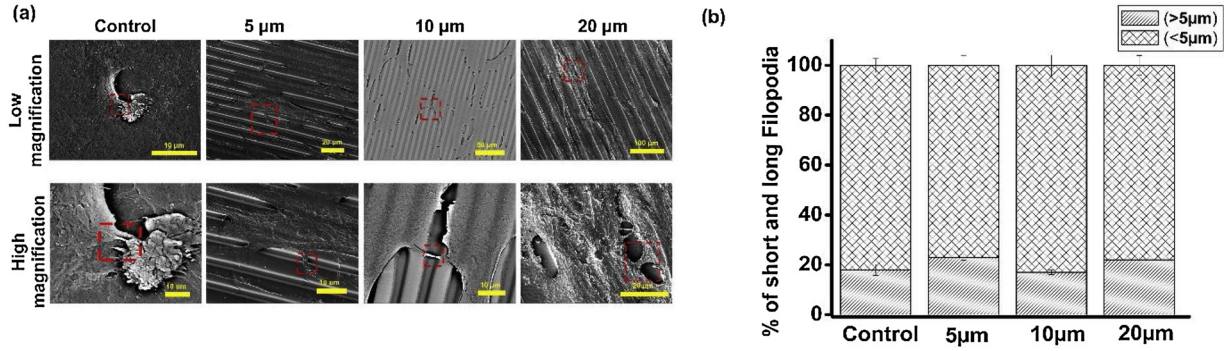

Fig. 5. (a) Representative SEM images (Low and high magnification) of filopodia on plain and different micropatterned PDMS substrate. Filopodia kept straight (plain surface) or bent (micropatterned surface) to follow the pattern contour (denoted by red dotted box) (b) Stacked histograms reporting the fraction of short (less than 5 μm, red columns) and long (more than 5 μm, black columns) filopodia on plain and the micropatterned substrates. (For interpretation of the references to colour in the Figure, the reader is referred to the web version of this article).

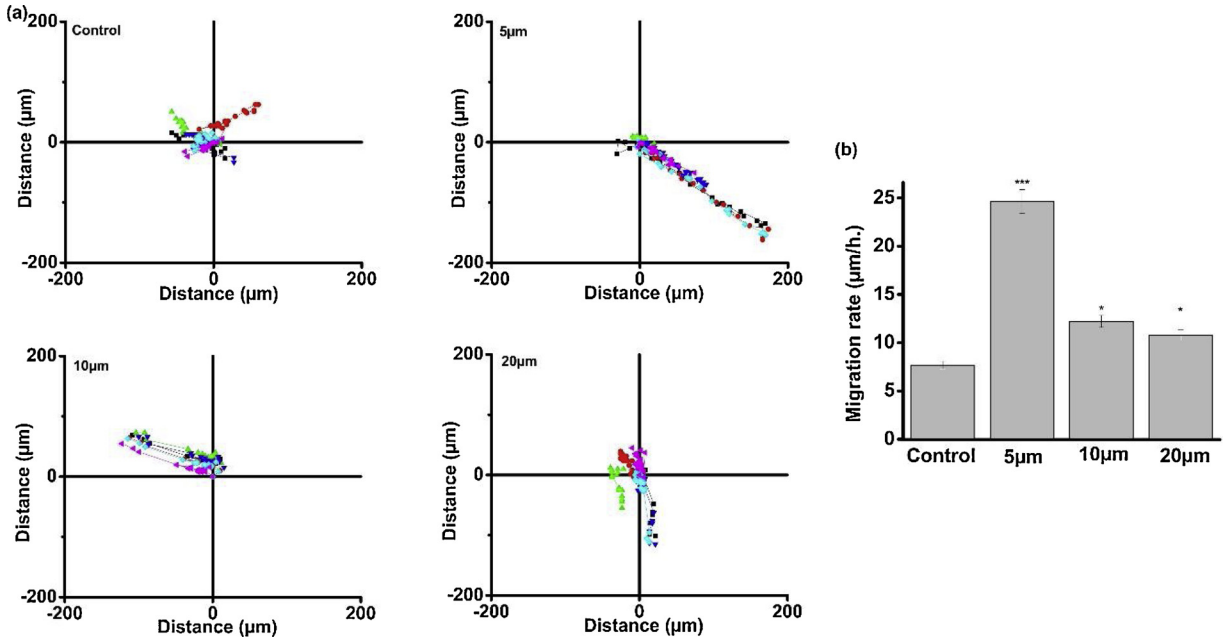

Fig. 6. Migration rates of keratocytes cultured on the plain and micropatterned substrates. (a) Trajectories of six cells cultured on the plain or micropatterned substrates. Cells were imaged at 15 min intervals for 6 h. (b) Mean migration rates of cells cultured on each surface (n = 6 cells per surface). Values represented as mean ± SD. The mean migration rate of cells cultured on 5 μm patterned surface was significantly higher than those of cells cultured on plain substrates ($p < 0.001$).

Immunofluorescent staining was used to detect molecules associated with native keratocyte and myofibroblastic cell types (Supplemental Fig. 4). Cells on all the substrates exhibited the keratocyte markers ALDH3A1 and keratocan. None of the substrates showed any detectable levels of αSMA, a myofibrotic marker.

4. Discussions

In this study, the presence of microgrooves on a substrate, ranging in size from 5 to 20 μm, were shown to influence the behaviour of corneal keratocytes. The micropatterned substrates mimic the parallel orientation of fibrils in each lamella of the stroma. A high percentage of keratocytes in the study aligned along the microgroove patterns implying that the cells could recognize orthotropic topographic stimuli [5]. Focal adhesion, stress fibers, orientation, migration and phenotype were all influenced by the surface topography.

The cells stress fibers and FAs were mostly aligned with the patterned topography in this study. It has previously been shown that nanoscale features in the topography partially inhibited FAs and stress fibers while they are abundant on substrates presenting microscale topography [5]. The current work shows that geometrical confinement, induced due to topographically patterned microgroove substrates modulated cell and nuclear morphology, along with such cellular behavior as alignment, orientation and migration. These factors are important for several biological phenomenon, including, embryogenesis, wound healing, metastasis, inflammation, and colonization of biomaterial scaffolding [22]. Topographic constraints led to significant squeezing of cells and nuclei, chromatin condensation – leading to changed cell proliferation rate – and cytoskeleton reorganization. Smaller groves (5 μm) on substrates had the most F-actin expression in cells compared to cells cultured on substrates with larger grooves (10 or 20 μm).

Cells grown on all the micropatterned substrates had significantly smaller nuclei and cell size, compared to the controls, which were devoid of any patterns. Previous studies have suggested that deformation of nuclei results from change to the cells morphology [11,46]. In addition, we observed that cells on micropatterned substrates expanded more quickly than the cells on the control substrate. Cell cycle times have previously been shown to be shorter in smaller sized cells than the average cells [35], which is in line with our findings.

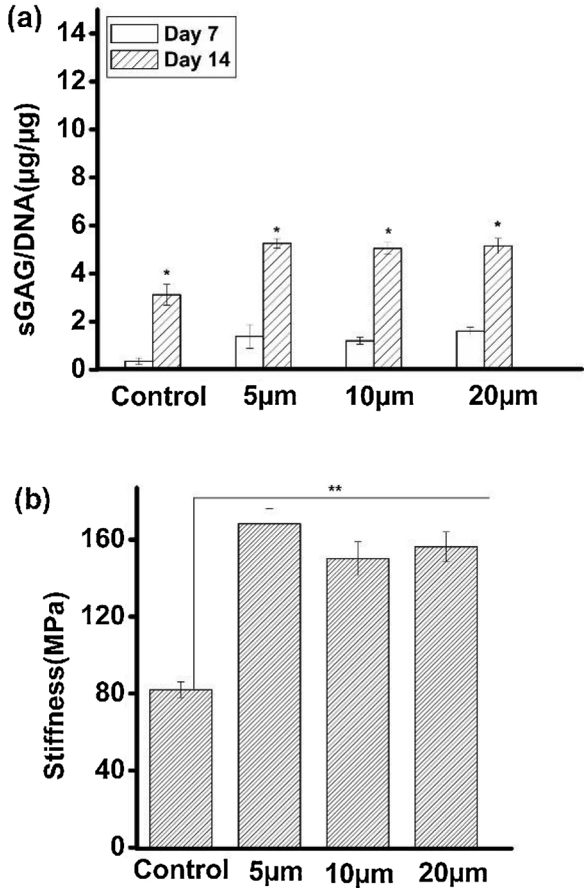

Fig. 7. (a) sGAG/DNA after 7 and 14 days of culture. (b) Significant difference ($p < 0.01$) in matrix stiffness between plain and micropatterned substrates was recorded after 7 days.

Despite their limited motility, keratocytes can actively probe their surroundings using filopodial. The cells can "sense" their environment through lamellipodial and filopodial extensions along the surface. Through interconnections among them, they form a cellular syncytium [47,48]. The filopodial extensions were mostly aligned along the pattern on the substrates. This in part explain why 5 µm substrates had the highest cellular migration rates. Filopodial probing is closely related to filopodia length. As features at a greater distance than filopodia length cannot be reached, new FAs cannot be formed. Herein comes the role of topographical cues. If topographic features' spacing is smaller than filopodial lengths, establishing fresh points of focal adhesion becomes easier for the cell. Growth of FAs, in turn, influences cell adhesion and polarization. The microgrooves have the potential to affect filopodial sensing and adhesion. Existing literature provides average filopodial dimensions to be 1–5 µm [20]. From the results in the current study, it may be observed that the dimensions of filopodia are similar on micropatterned surfaces.

Substrate topography can effectively influence cell proliferation, adhesion, and migration [49,26]. A barrier to moving towards cell control *via* topography is our limited understanding of the fundamentals behind cell-topography interaction. For better comprehension of how cells interact with topographical cues, microgroove substrates were used, with grooves at a scale that could interfere with cell filopodial probing and the establishment and growth of focal adhesions.

FA formation follows filopodial probing. The subsequent extension of the adhesions may be obstructed by the topographic patterns [50]. It may be observed here that filopodial dimensions are long enough to reach the valleys formed by the grooves. This would not preclude the formation of new FAs inside the grooves. However, FAs were primarily formed on the ridges. As observed by Albuschies & Vogel, for high angles between filopodia and adhesion surface (exceeding 12° on glass) FA formation is not favoured [51]. This could be due to the higher normal stress on a filopodial extension when the angle increases, thus disrupting integrin-ligand complex. It is conceivable that filopodia trying to reach the bottom of grooves would be subjected to similar high angles with respect to the adhesion surface, implying the preferred spots of FAs would be limited to ridge tops. The topographic cues could also ensure their presence in specific areas on the substrate.

Among the fabricated patterns, those with the 5 µm grooves were more favourable for formation of FAs on the ridges. This is likely due to the smaller aspect ratio of the patterns in this particular substrate. In concurrence with previous reports, the ordered topographical patterns altered cell migration and spread [52,53]. The elongation was highest for the 5 µm pattern substrates and cells displayed better alignment with the pattern direction. Migration direction was in close correspondence with the pattern direction. Lengthened FAs were aligned along the patterns. For the 5 and 10 µm patterned substrates, a fraction of the FAs were directed normal to the pattern instead of being parallel. FA behavior was remarkably different for the 20 µm pattern substrate. They were isolated, occupied ridge or groove patterns only partially, and the connected actin fibers were more like uncontracted dorsal stress fibers 53].

Transverse adhesions were possible on the substrate with 5 µm dimension patterns. When an FA is constrained due to geometry and is not able to grow in proportion to the tensile forces, the resistance reduces in the transverse direction to compensate [54]. This implies that adhesions along the transverse direction are more likely to unravel. Adhesions that can elongate along the ridge are more likely to be stable. Hence, this leads to cell elongation and increased migration along the direction of the patterns. Thus, the results suggest that surface topography can be used to direct cell culture migration, *i.e.*, patterns at the micro-scale influenced the whole cell sheet cell growth [55].

Increased ALDH3A1, keratocan, decorin and lumican expression by cells on the substrates with the microgrooves supports the idea that aligned topographical cues promote a keratocyte phenotype. This agrees with previous studies that show alignment can up-regulate the expression of keratocyte related genes [56,57]. Increases were also noted for the gene expression of collagen types I, III and V. These collagens make up a significant proportion of the corneal ECM. Collagen type I is the most abundant collagen found in the stroma, mostly in the fibrils. Interactions between collagens I and V result in heteropolymeric fibril formation and regulation of fibril diameter [24]. While collagen III is present in the healthy cornea, it is normally up regulated in keratocytes after injury [58]. This would seem to imply that keratocytes were partially activated to promote wound healing by the microgrooves but were still exhibiting markers associated with a quiescent keratocyte.

Corneal transparency is the results of the highly structured stromal ECM and the presence of intracellular crystallins in the keratocytes [47]. ALDH3A1 is one of the more prominent crystallin proteins expressed by keratocytes. Its expression was up regulated by cells on micropatterned surfaces, with expression levels increasing as pattern size reduced. In the non-patterned substrates, only low levels of mRNA expression were noted. The topographic cues played a role in regulating ALDH3A1 expression. The cytoskeletal reorganization caused by the surface microstructure likely led to the alteration in gene expression [24].

5. Conclusion

The current work was able to demonstrate that fundamental cell behaviors of keratocytes – shape, alignment, and migration – could be guided by just the environmental topography. The topographical cues also affected cell and nuclear morphology as well as collective cell growth. Cell morphology and nucleus deformation as a result of

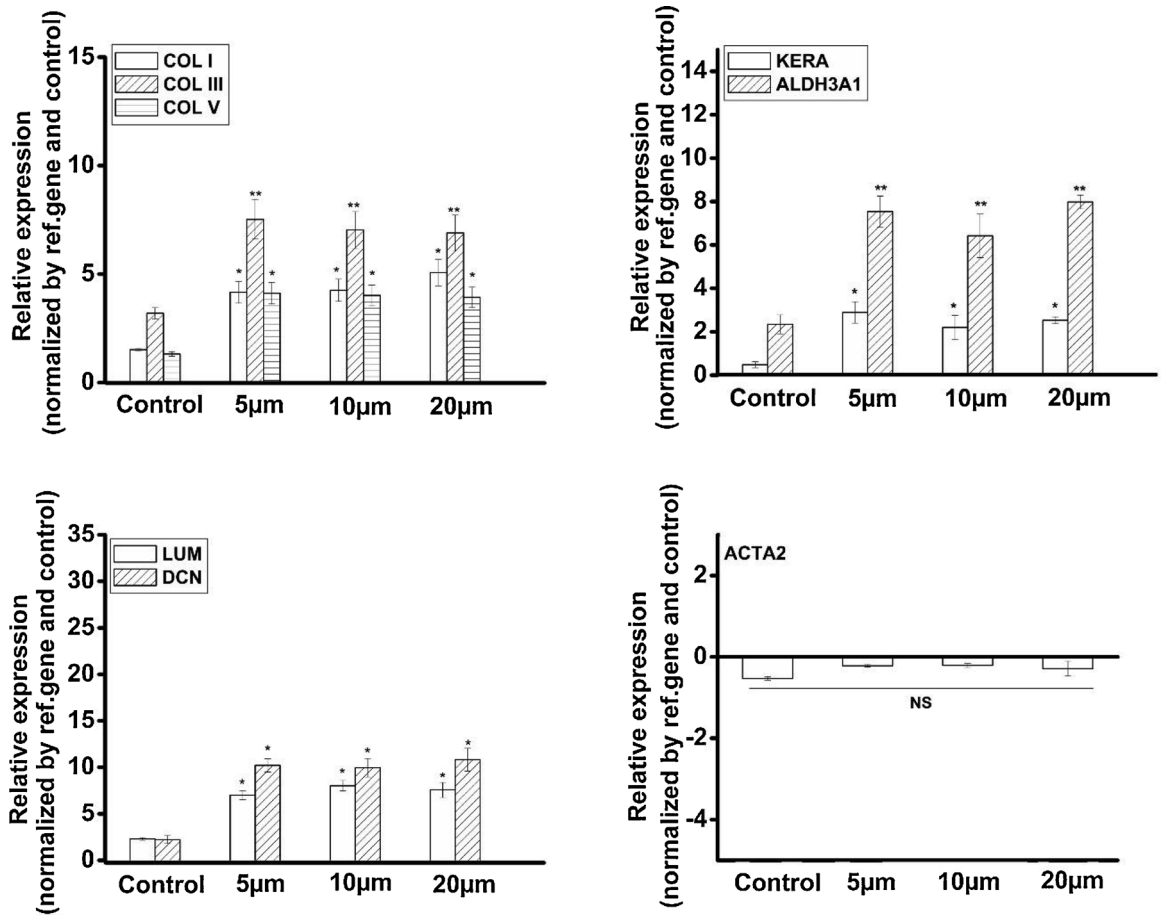

Fig. 8. Fold change gene expression analysis of ECM markers COLI, COLIII, COLV, corneal keratocyte-specific markers KERA, ALDH3A1, LUM and DCN and myofibroblasts specific marker αSMA (ACTA2). Quantification done by rtPCR (n(= 3) ± SD). ***p < 0.001, **p < 0.01 and *p < 0.05, One-way ANOVA, followed by Tukey's Honest significant difference test.

topographical cues was accompanied by significant cytoskeletal reorganization and chromatin condensation. As well as providing insight into how keratocytes are regulated by their microenvironment, these findings could be applied to assist in controlling how the cells behave when engineering corneal stromal tissue *in vitro*.

Author contribution statement

- Promita Bhattacharjee conducted experiments, analyzed data and prepared the manuscript.
- Brenton L Cavanagh conducted live cell imaging.
- Mark Ahearne planned and supervised the project and corrected the manuscript for publication.

Declaration of Competing Interest

The authors declare that they have no known competing financial interests or personal relationships that could have appeared to influence the work reported in this paper.

Acknowledgements

The research leading to these results has received funding from the European Research Council (ERC) under the European Union's Horizon 2020 research and innovation program (EYEREGEN - 637460) and from Science Foundation Ireland (15/ERC/3269).

Appendix A. Supplementary data

Supplementary material related to this article can be found, in the online version, at doi:https://doi.org/10.1016/j.colsurfb.2020.110971.

References

[1] G.A. Abrams, A.I. Teixeira, P.F. Nealey, C.J. Murphy, Effects of substratum topography on cell behavior, in: A. Dillow, A. Lowman (Eds.), Biomimetic Materials and Design, CRC Press, Boca Raton, 2002, pp. 97–125.
[2] R. Sridharan, B. Cavanagh, A.R. Cameron, D.J. Kelly, F.J. O'Brien, Material stiffness influences the polarization state, function and migration mode of macrophages, Acta Biomater. (2019).
[3] R.G. Flemming, C.J. Murphy, G.A. Abrams, S.L. Goodman, P.F. Nealey, Effects of synthetic micro- and nano-structured surfaces on cell behavior, Biomaterials 20 (6) (1999) 573–588.
[4] J. Baek, S.Y. Cho, H. Kang, H. Ahn, W.B. Jung, Y. Cho, E. Lee, S.W. Cho, H.T. Jung, S.G. Im, Distinct mechanosensing of human neural stem cells on extremely limited anisotropic cellular contact, ACS Appl. Mater. Interfaces 10 (40) (2018) 33891–33900.
[5] A.I. Teixeira, P.F. Nealey, C.J. Murphy, Responses of human keratocytes to micro- and nanostructured substrates, J. Biomed. Mater. Res. A. 71a (3) (2004) 369–376.
[6] S. Kondo, T. Miura, Reaction-diffusion model as a framework for understanding biological pattern formation, Science 329 (5999) (2010) 1616–1620.
[7] W.F. Marshall, Differential Geometry Meets the Cell, Cell 154 (2) (2013) 265–266.
[8] M. Thery, Micropatterning as a tool to decipher cell morphogenesis and functions, J. Cell. Sci. 123 (24) (2010) 4201–4213.
[9] G. Charras, E. Sahai, Physical influences of the extracellular environment on cell migration, Nat. Rev. Mol. Cell Biol. 15 (12) (2014) 813–824.
[10] J.B. Moseley, P. Nurse, Cell division intersects with cell geometry, Cell 142 (2) (2010) 189–193.
[11] M. Versaevel, T. Grevesse, S. Gabriele, Spatial coordination between cell and nuclear shape within micropatterned endothelial cells, Nat. Commun. 3 (2012).
[12] C.S. Chen, M. Mrksich, S. Huang, G.M. Whitesides, D.E. Ingber, Geometric control of cell life and death, Science 276 (5317) (1997) 1425–1428.

[13] M. Lunova, V. Zablotskii, N.M. Dempsey, T. Devillers, M. Jirsa, E. Sykova, S. Kubinova, O. Lunov, A. Dejneka, Modulation of collective cell behaviour by geometrical constraints, Integr. Biol. 8 (11) (2016) 1099–1110.
[14] Y. Li, J.S. Chu, K. Kurpinski, X. Li, D.M. Bautista, L. Yang, K.L.P. Sung, S. Li, Biophysical regulation of histone acetylation in mesenchymal stem cells, Biophys. J. 100 (8) (2011) 1902–1909.
[15] A.J. Engler, S. Sen, H.L. Sweeney, D.E. Discher, Matrix elasticity directs stem cell lineage specification, Cell 126 (4) (2006) 677–689.
[16] L.E. McNamara, R. Burchmore, M.O. Riehle, P. Herzyk, M.J.P. Biggs, C.D.W. Wilkinson, A.S.G. Curtis, M.J. Dalby, The role of microtopography in cellular mechanotransduction, Biomaterials 33 (10) (2012) 2835–2847.
[17] K.A. Kilian, B. Bugarija, B.T. Lahn, M. Mrksich, Geometric cues for directing the differentiation of mesenchymal stem cells, Proc. Natl. Acad. Sci. U.S.A. 107 (11) (2010) 4872–4877.
[18] A. Graziano, R. d'Aquino, M.G. Cusella-De Angelis, G. Laino, A. Piattelli, M. Pacifici, A. De Rosa, G. Papaccio, Concave pit-containing scaffold surfaces improve stem cell-derived osteoblast performance and lead to significant bone tissue formation, PLoS One 2 (6) (2007).
[19] Y.B. Sun, C.S. Chen, J.P. Fu, Forcing stem cells to behave: a biophysical perspective of the cellular microenvironment, Annu. Rev. Biophys. 41 (41) (2012) 519–542.
[20] M. Ventre, C.F. Natale, C. Rianna, P.A. Netti, Topographic cell instructive patterns to control cell adhesion, polarization and migration, J. R. Soc. Interface 11 (100) (2014).
[21] M. Ventre, F. Causa, P.A. Netti, Determinants of cell-material crosstalk at the interface: towards engineering of cell instructive materials, J. R. Soc. Interface 9 (74) (2012) 2017–2032.
[22] S.A. Pot, S.J. Liliensiek, K.E. Myrna, E. Bentley, J.V. Jester, P.F. Nealey, C.J. Murphy, Nanoscale topography-induced modulation of fundamental cell behaviors of rabbit corneal keratocytes, fibroblasts, and myofibroblasts, Invest. Ophthalmol. Vis. Sci. 51 (3) (2010) 1373–1381.
[23] K.M. Meek, C. Knupp, Corneal structure and transparency, Prog. Retin. Eye Res. 49 (2015) 1–16.
[24] S. Koo, S.J. Ahn, H. Zhang, J.C. Wang, E.K.F. Yim, Human corneal keratocyte response to Micro- and nano-gratings on chitosan and PDMS, Cell. Mol. Bioeng. 4 (3) (2011) 399–410.
[25] S.J. Liliensiek, S. Campbell, P.F. Nealey, C.J. Murphy, The scale of substratum topographic features modulates proliferation of corneal epithelial cells and corneal fibroblasts, J. Biomed. Mater. Res. Part A 79 (1) (2006) 185–192.
[26] W. Zhang, J.L. Chen, L.J. Backman, A.D. Malm, P. Danielson, Surface Topography and Mechanical Strain Promote Keratocyte Phenotype and Extracellular Matrix Formation in a Biomimetic 3D Corneal Model, Adv. Healthc. Mater. 6 (5) (2017).
[27] A.I. Teixeira, G.A. Abrams, P.J. Bertics, C.J. Murphy, P.F. Nealey, Epithelial contact guidance on well-defined micro- and nanostructured substrates, J. Cell. Sci. 116 (10) (2003) 1881–1892.
[28] J. Fernandez-Perez, M. Ahearne, Influence of biochemical cues in human corneal stromal cell phenotype, Curr. Eye Res. 44 (2) (2019) 135–146.
[29] A.M. Lipski, C.J. Pino, F.R. Haselton, I.W. Chen, V.P. Shastri, The effect of silica nanoparticle-modified surfaces on cell morphology, cytoskeletal organization and function, Biomaterials 29 (28) (2008) 3836–3846.
[30] J. Schindelin, I. Arganda-Carreras, E. Frise, V. Kaynig, M. Longair, T. Pietzsch, S. Preibisch, C. Rueden, S. Saalfeld, B. Schmid, J.Y. Tinevez, D.J. White, V. Hartenstein, K. Eliceiri, P. Tomancak, A. Cardona, Fiji: an open-source platform for biological-image analysis, Nat. Methods 9 (7) (2012) 676–682.
[31] M. Maruoka, M. Sato, Y.F. Yuan, M. Ichiba, R. Fuji, T. Ogawa, N. Ishida-Kitagawa, T. Takeya, N. Watanabe, Abi-1-bridged tyrosine phosphorylation of VASP by Abelson kinase impairs association of VASP to focal adhesions and regulates leukaemic cell adhesion, Biochem. J. 441 (2012) 889–899.
[32] M. Ahearne, J. Lysaght, A.P. Lynch, Combined influence of basal media and fibroblast growth factor on the expansion and differentiation capabilities of adipose-derived stem cells, Cell Regen (Lond) 3 (1) (2014) 13.
[33] Y.J. Kim, R.L.Y. Sah, J.Y.H. Doong, A.J. Grodzinsky, Fluorometric assay of DNA in cartilage explants using Hoechst-33258, Anal. Biochem. 174 (1) (1988) 168–176.
[34] C. Roduit, S. Sekatski, G. Dietler, S. Catsicas, F. Lafont, S. Kasas, Stiffness tomography by atomic force microscopy, Biophys. J. 97 (2) (2009) 674–677.
[35] F.B. Gao, M. Raff, Cell size control and a cell-intrinsic maturation program in proliferating oligodendrocyte precursor cells, J. Cell Biol. 138 (6) (1997) 1367–1377.
[36] V. Vogel, M. Sheetz, Local force and geometry sensing regulate cell functions, Nat. Rev. Mol. Cell Biol. 7 (4) (2006) 265–275.
[37] G. Halder, S. Dupont, S. Piccolo, Transduction of mechanical and cytoskeletal cues by YAP and TAZ, Nat. Rev. Mol. Cell Biol. 13 (9) (2012) 591–600.
[38] M.P. Murrell, M.L. Gardel, F-actin buckling coordinates contractility and severing in a biomimetic actomyosin cortex, Proc. Natl. Acad. Sci. U.S.A. 109 (51) (2012) 20820–20825.
[39] R. McBeath, D.M. Pirone, C.M. Nelson, K. Bhadriraju, C.S. Chen, Cell shape, cytoskeletal tension, and RhoA regulate stem cell lineage commitment, Dev. Cell 6 (4) (2004) 483–495.
[40] G. Mascetti, L. Vergani, A. Diaspro, S. Carrara, G. Radicchi, C. Nicolini, Effect of fixatives on calf thymocytes chromatin as analyzed by 3D high-resolution fluorescence microscopy, Cytometry 23 (2) (1996) 110–119.
[41] L. Vergani, M. Grattarola, C. Nicolini, Modifications of chromatin structure and gene expression following induced alterations of cellular shape, Int. J. Biochem. Cell Biol. 36 (8) (2004) 1447–1461.
[42] N. Minc, D. Burgess, F. Chang, Influence of Cell Geometry on Division-Plane Positioning, Cell 144 (3) (2011) 414–426.
[43] M. Thery, V. Racine, M. Piel, A. Pepin, A. Dimitrov, Y. Chen, J.B. Sibarita, M. Bornens, Anisotropy of cell adhesive microenvironment governs cell internal organization and orientation of polarity, Proc. Natl. Acad. Sci. U.S.A. 103 (52) (2006) 19771–19776.
[44] Y.T. Zhang, A.H. Conrad, G.W. Conrad, Effects of Ultraviolet-A and Riboflavin on the interaction of collagen and proteoglycans during corneal cross-linking, J. Biol. Chem. 286 (15) (2011) 13011–13022.
[45] L.T.Y. Ho, A.M. Harris, H. Tanioka, N. Yagi, S. Kinoshita, B. Caterson, A.J. Quantock, R.D. Young, K.M. Meek, A comparison of glycosaminoglycan distributions, keratan sulphate sulphation patterns and collagen fibril architecture from central to peripheral regions of the bovine cornea, Matrix Biol. 38 (2014) 59–68.
[46] N. Jain, K.V. Iyer, A. Kumar, G.V. Shivashankar, Cell geometric constraints induce modular gene-expression patterns via redistribution of HDAC3 regulated by actomyosin contractility, Proc. Natl. Acad. Sci. U.S.A. 110 (28) (2013) 11349–11354.
[47] J.V. Jester, P.A. Barry, G.J. Lind, W.M. Petroll, R. Garana, H.D. Cavanagh, Corneal keratocytes - in-situ and in-vitro organization of cytoskeletal contractile proteins, Invest. Ophthalmol. Vis. Sci. 35 (2) (1994) 730–743.
[48] T. Nishida, K. Yasumoto, T. Otori, J. Desaki, The network structure of corneal fibroblasts in the rat as revealed by scanning electron-microscopy, Invest. Ophthalmol. Vis. Sci. 29 (12) (1988) 1887–1890.
[49] B.D. Lawrence, J.K. Marchant, M.A. Pindrus, F.G. Omenetto, D.L. Kaplan, Silk film biomaterials for cornea tissue engineering, Biomaterials 30 (7) (2009) 1299–1308.
[50] C.F. Natale, M. Ventre, P.A. Netti, Tuning the material-cytoskeleton crosstalk via nanoconfinement of focal adhesions, Biomaterials 35 (9) (2014) 2743–2751.
[51] J. Albuschies, V. Vogel, The role of filopodia in the recognition of nanotopographies, Sci. Rep. 3 (2013).
[52] E.T. den Braber, J.E. de Ruijter, L.A. Ginsel, A.F. von Recum, J.A. Jansen, Orientation of ECM protein deposition, fibroblast cytoskeleton, and attachment complex components on silicone microgrooved surfaces, J. Biomed. Mater. Res. 40 (2) (1998) 291–300.
[53] S. Tojkander, G. Gateva, G. Schevzov, P. Hotulainen, P. Naumanen, C. Martin, P.W. Gunning, P. Lappalainen, A molecular pathway for myosin II recruitment to stress fibers, Curr. Biol. 21 (7) (2011) 539–550.
[54] N.Q. Balaban, U.S. Schwarz, D. Riveline, P. Goichberg, G. Tzur, I. Sabanay, D. Mahalu, S. Safran, A. Bershadsky, L. Addadi, B. Geiger, Force and focal adhesion assembly: a close relationship studied using elastic micropatterned substrates, Nat. Cell Biol. 3 (5) (2001) 466–472.
[55] B.D. Lawrence, Z. Pan, M.I. Rosenblatt, Silk film topography directs collective epithelial cell migration, PLoS One 7 (11) (2012).
[56] S.L. Wilson, I. Wimpenny, M. Ahearne, S. Rauz, A.J. El Haj, Y. Yang, Chemical and topographical effects on cell differentiation and matrix elasticity in a corneal stromal layer model, Adv. Funct. Mater. 22 (17) (2012) 3641–3649.
[57] K.Y. Then, Y. Yang, M. Ahearne, A.J. El Haj, Effect of microtopographical cues on human keratocyte orientation and gene expression, Curr. Eye Res. 36 (2) (2011) 88–93.
[58] Y. Qazi, G. Wong, B. Monson, J. Stringham, B.K. Ambati, Corneal transparency: genesis, maintenance and dysfunction, Brain Res. Bull. 81 (2–3) (2010) 198–210.